

SUPPLEMENTAL MATERIAL

Manipulating ultrafast magnetization dynamics of ferromagnets using the odd-even layer of two-dimensional transition metal di-chalcogenides

Soma Dutta,^a Sajid Husain,^{*b} Prabhat Kumar,^c Nanhe Kumar Gupta,^d Sujeet Chaudhary,^d

Peter Svedlindh,^b and Anjan Barman,^{*a}

^aDepartment of Condensed Matter and Materials Physics, S. N. Bose National Centre for Basic Sciences, Block JD, Sector-III, Salt Lake, Kolkata 700 106, India. Email: abarman@bose.res.in

^bDepartment of Materials Science and Engineering, Uppsala University, Box 35, SE-751 03 Uppsala, Sweden. Email: shusain@lbl.gov

^cDepartment of Thin Films and Nanostructures, Institute of Physics of the Czech Academy of Sciences, Cukrovarnická 10/112, 162 00 Prague, Czech Republic

^dThin Film Laboratory, Department of Physics, Indian Institute of Technology Delhi, New Delhi 110016, India

Static Characterization:

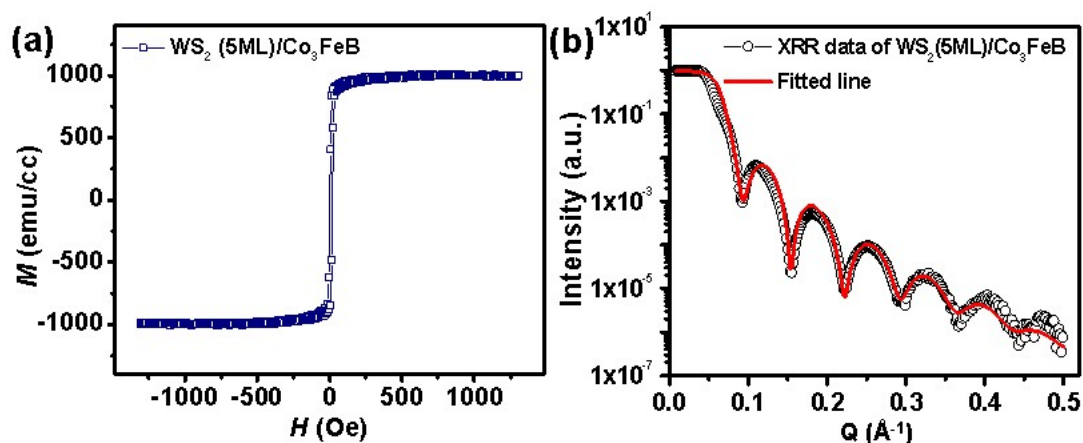


Figure S1. (a) Static in-plane magnetic hysteresis loop and (b) x-ray reflectivity spectrum from WS₂ (5 ML)/Co₃FeB (6 nm) heterostructure.

A room temperature in-plane (IP) magnetic hysteresis loop of the WS₂ (5 ML)/Co₃FeB heterostructure, measured using vibrating sample magnetometry (VSM) (Quantum Design PPMS, Dynacool-9T system), is shown in Fig. S1(a). The small value of the saturation field is evidence of an IP magnetic easy axis with negligible OOP configuration. The small value of the coercive field, $H_c \sim 1.4$ Oe indicates the soft ferromagnetic nature of the heterostructure.

Fig. S1(b) shows the x-ray reflectivity (XRR) spectrum of WS₂ (5 ML)/Co₃FeB heterostructure measured using a 1.54 Å Cu-K α x-ray source. The XRR spectrum exhibits

well defined oscillations up to a scattering vector of 0.5 \AA^{-1} signifying uniform deposition. The ‘Reflex’ software was used to analyze the XRR spectra from where we have extracted the thickness, scattering length density (SLD) and roughness of the different layers. The SLD is proportional to the electron density of the material. The values of the layer thicknesses obtained from the fits are found to be close to their nominal thickness values. The interfacial roughness and SLD obtained from the fits are tabulated in Table 1.

Table S1: Parameters obtained from the XRR analysis of WS_2 (n_{ML})/ Co_3FeB heterostructures.

Heterostructure	Layer	Thickness (nm)	Roughness (nm)	SLD (10^{-5} \AA^{-2})
Co_3FeB	Al	5.5	1.1	2.635
	Co_3FeB	6.3	0.5	8.087
	Sub	-	0.17	2.067
$\text{WS}_2(1\text{ML})/\text{Co}_3\text{FeB}$	Al	5.1	1.2	2.112
	Co_3FeB	6.2	0.3	8.588
	WS_2	1	0.4	4.817
	Sub	-	0.9	2.014
$\text{WS}_2(2\text{ML})/\text{Co}_3\text{FeB}$	Al	4	0.4	2.112
	Co_3FeB	8	0.4	8.588
	WS_2	1.8	0.3	4.066
	Sub	-	1.9	2.014
$\text{WS}_2(3\text{ML})/\text{Co}_3\text{FeB}$	Al	4.6	0.9	2.379
	Co_3FeB	8	0.4	8.85
	WS_2	2.8	0.2	4.434
	Sub	-	0.3	2.492
$\text{WS}_2(4\text{ML})/\text{Co}_3\text{FeB}$	Al	4.3	0.38	2.635
	Co_3FeB	4.7	0.1	8.088
	WS_2	3.8	0.3	7.15
	Sub	-	0.45	2.067
$\text{WS}_2(5\text{ML})/\text{Co}_3\text{FeB}$	Al	4	1.12	2.635
	Co_3FeB	4.2	0.3	6.869
	WS_2	4.44	1.3	7.15
	Sub	-	0.57	2.067

Raman Spectroscopy:

Raman spectroscopy has been performed to accurately identify the number of WS_2 layers using a solid-state laser based LABRAM HR Evolution instrument with 600 lines/mm spectral resolution. We used 532 nm laser excitations, keeping the laser power 1.15 mW at all times. A_{1g} mode blueshifts with the increase of WS_2 layer number that is consistent with the increase of restoring force caused by the interlayer van der Waals interactions. The low intensity peak at low wavenumber corresponds to the out-of-plane acoustic phonon mode. The blueshift of A_{1g} and redshift of E_{2g} are the proof of the formation of 1, 2, 3, 4, 5 ML. Observation of Raman peaks in all samples is indicative of the crystalline nature of WS_2 .

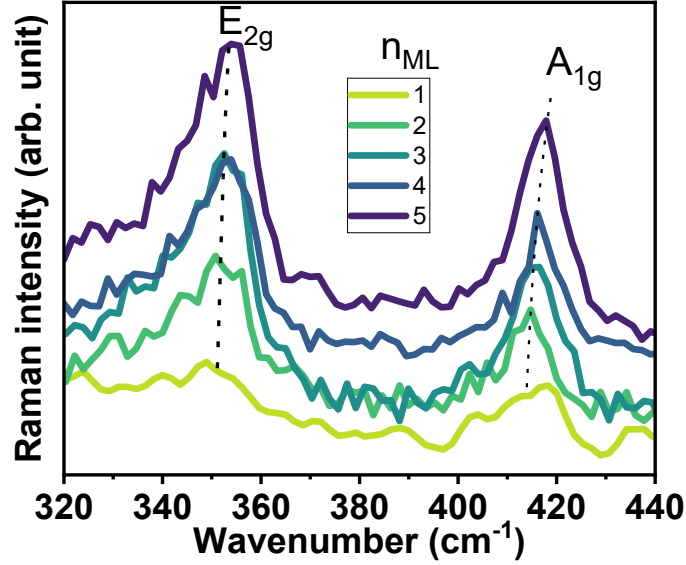


Figure S2. Raman spectra of WS₂ for 1 - 5 layers. Dotted lines indicate the peak shift with layer numbers.

Layer dependent slow remagnetization time

The slow remagnetization time is the time (τ_1) to dissipate heat across the temperature gradient from ferromagnet to substrate via WS₂. Variation of τ_1 on odd-even layer numbers of WS₂ is shown in Fig. S3

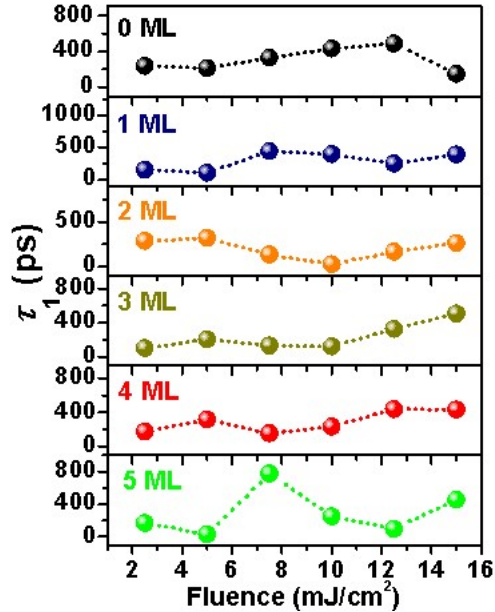


Figure S3. Variation of τ_1 with pump fluence for different number of layers of WS₂.

Experimental and numerical studies have shown that thermal transport in TMDs is phonon mediated.¹ The lattice specific heat (C_p) and thermal conductivity (κ) play dominant roles for thermal time constant in thermal dissipation. It is notable that both the in-plane (IP) and cross-plane κ contribute for this kind of layered materials.² While the IP κ increases with WS₂ layer number and helps for heat dissipation, cross-plane κ hinders the vertical heat flow

due to the weak interlayer van der Waals interaction. Due to the balancing between IP and cross-plane κ , we have not observed any layer dependence of slow remagnetization time.

Three Temperature Modelling of Ultrafast Demagnetization

We have modelled the experimental ultrafast demagnetization data of Co₃FeB (6 nm) thin film obtained from TR-MOKE magnetometry at different pump fluences using three-temperature modelling (3TM). The three coupled differentail equations can be written as:

$$C_e(T_e)\frac{dT_e}{dt} = -G_{el}(T_e - T_l) - G_{es}(T_e - T_s) + P(t) \quad (\text{S1a})$$

$$C_s(T_s)\frac{dT_s}{dt} = -G_{sl}(T_s - T_l) - G_{es}(T_s - T_e) \quad (\text{S1b})$$

$$C_l(T_l)\frac{dT_l}{dt} = -G_{sl}(T_l - T_s) - G_{el}(T_l - T_e) \quad (\text{S1c})$$

Where C_e , C_s and C_l are the electron, spin and lattice specific heats. Electronic specific heat is proportional to the electron temperature, i.e., $C_e = \gamma T_e$, where $\gamma = 0.7 \times 10^3 \text{ Jm}^{-3}\text{K}^{-1}$. T_e , T_s and T_l are temperature of electron, spin and lattice bath, respectively. Initial temperatures are kept at room temperature, i.e., 300 K. G_{el} , G_{es} and G_{sl} are the electron-lattice, electron-spin and spin-lattice coupling strength constant. Initial electronic excitation is expressed by adding the laser source term, $P(t)$ to Eq. S1a only. The temporal evolution of the spin temperature is then fed into the mean field theory to reproduce the similar change in magnetization that is observed in the experiment. Curie temperature (T_c) of Co₃FeB is $\sim 1313 \text{ K}$.³

We have enlisted the value of absorbed energy (E_a) and rise of electronic temperatures (T_e) using Eq. 5 and 6 of the manuscript and different parameters obtained from 3TM at different pump fluences for Co₃FeB (6 nm) thin film in Table 2 below.

Table S2: Estimation of different parameters obtained from Eq. 5, 6 and 3TM for Co₃FeB (6 nm) film.

F (mJ/cm ²)	E _a (mJ/cc)	T _e (K)	C _l (× 10 ⁶ Jm ⁻³ K ⁻¹)	C _s (× 10 ⁶ Jm ⁻³ K ⁻¹)	G _{el} (× 10 ¹⁷ Wm ⁻³ K ⁻¹)	G _{es} (× 10 ¹⁷ Wm ⁻³ K ⁻¹)	G _{sl} (× 10 ¹⁷ Wm ⁻³ K ⁻¹)
2.5	0.67×10 ⁶	1416	3.8	2.3	7	29.2	8
5	1.34×10 ⁶	1979	4.2	3.5	6	29	13
7.5	2.01×10 ⁶	2415	4.5	3.68	6	28.5	14
10	2.67×10 ⁶	2778	5.3	3.8	11	28	10
12.5	3.34×10 ⁶	3104	5.5	3.95	11	27	12.5
15	4.01×10 ⁶	3398	7	4.05	14	26	9

We have observed an increase in both C_l and C_s with pump fluence that corresponds to the rise of their respective bath temperatures. G_{es} is showing a decreasing trend with fluence indicating that the higher fluence weakens the strength of coupling between electron and spin followed by an increase in τ_m .

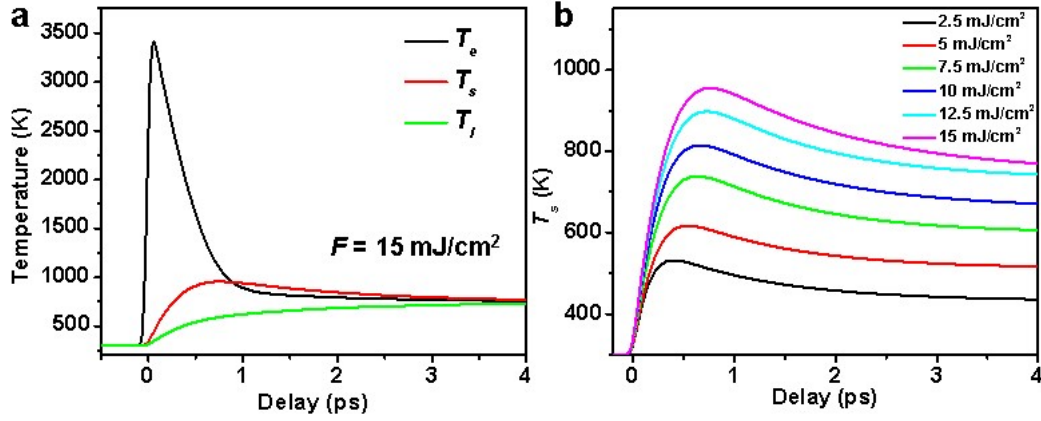


Figure S4. (a) Temporal evolution of electron temperature (T_e), spin temperature (T_s) and lattice temperature (T_l) at 15 mJ/cm^2 fluence and (b) variation of T_s as a function of time delay at different pump fluence for Co_3FeB (6 nm) thin film.

Variation of damping (α) and ultrafast demagnetization time (τ_m) with fluence

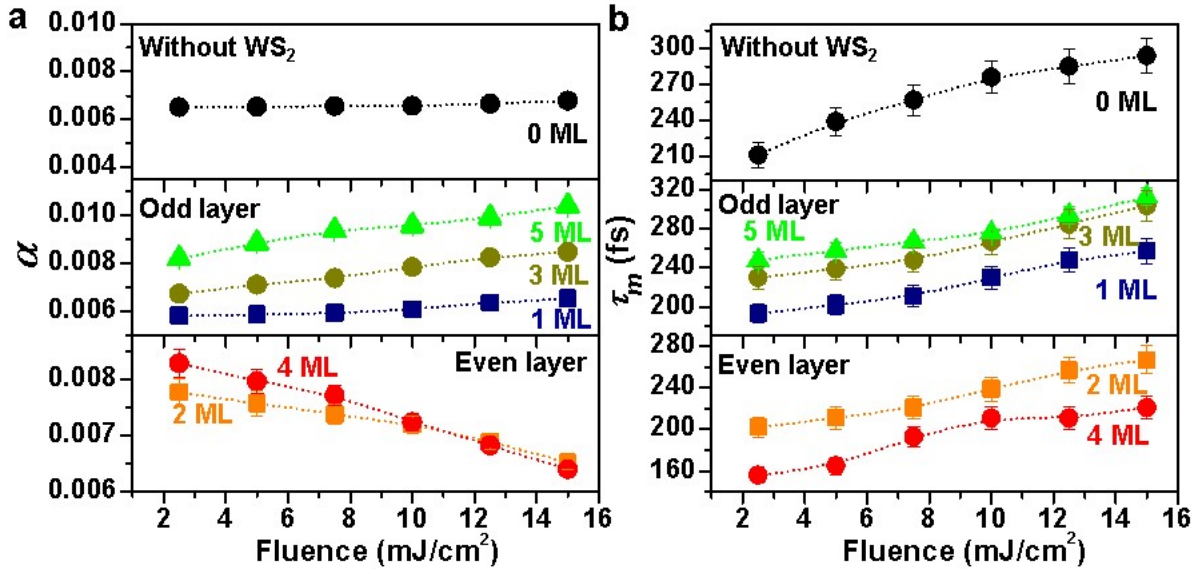


Figure S5. Variation of (a) α and (b) τ_m with pump fluences in absence of WS_2 , and for odd and even number of layers of WS_2 .

References:

1. S. E. Kim, F. Mujid, A. Rai, F. Eriksson, J. Suh, P. Poddar, A. Ray, C. Park, E. Fransson, Y. Zhong, D. A. Muller, P. Erhart, D. G. Cahill and J. Park, *Nature*, 2021, **597**, 660-665.
2. S. Mondal, Y. Lin, D. Polley, C. Su, A. Zettl, S. Salahuddin and J. Bokor, *ACS Nano*, 2022, **16**, 9620-9630.
3. B. Teso, S. Kravenkit, K. Sorn-in, A. Kaewrawang, A. Kruesubthaworn, A. Siritaratiwat, T. Mewes, C. K. A. Mewes and C. Surawanitkun, *Applied Surface Science*, 2019, **472**, 36-39.